EFDA–JET–CP(12)02/04

M. Groth, S. Brezinsek, P. Belo, G. Corrigan, D. Harting, S. Wiesen,
M.N.A Beurskens, M. Brix, M. Clever, J.W. Coenen, T. Eich, J. Flanagan,
C. Giroud, A. Huber, S. Jachmich, U. Kruezi, M. Lehnen, C. Lowry,
C.F. Maggi, S. Marsen, A.G. Meigs, G. Sergienko, B. Sieglin, C. Silva,
A. Sirinelli, M.F. Stamp, G.J. van Rooij,
and JET EFDA contributors

Target Particle and Heat Loads in Low-Triangularity L-mode Plasmas in JET with Carbon and Beryllium/Tungsten Walls

Target Particle and Heat Loads in Low-Triangularity L-mode Plasmas in JET with Carbon and Beryllium/Tungsten Walls

M. Groth[1], S. Brezinsek[2], P. Belo[3], G. Corrigan[4], D. Harting[2], S. Wiesen[2], M.N.A Beurskens[4], M. Brix[4], M. Clever[2], J.W. Coenen[2], T. Eich[5], J. Flanagan[4], C. Giroud[4], A. Huber[2], S. Jachmich[6], U. Kruezi[2], M. Lehnen[2], C. Lowry[7], C.F. Maggi[5], S. Marsen[8], A.G. Meigs[4], G. Sergienko[2], B. Sieglin[5], C. Silva[4], A. Sirinelli[3], M.F. Stamp[3], G.J. van Rooij[9], and JET EFDA contributors*

JET-EFDA, Culham Science Centre, OX14 3DB, Abingdon, UK

[1]Aalto University, Association EURATOM-Tekes, Espoo, Finland
[2]Institute for Energy and Climate Research, Association EURATOM-FZJ Jülich, Germany
[3]Institute of Plasmas and Nuclear Fusion, Association EURATOM-IST, Lisbon, Portugal
[4]EURATOM-CCFE Fusion Association, Culham Science Centre, OX14 3DB, Abingdon, OXON, UK
[5]Max-Planck Institute for Plasma Physics, EURATOM- Association, Garching, Germany
[6]Association "EURATOM Belgium State", Laboratory for Plasma Physics, Brussels, Belgium
[7]EFDA Close Support Unit, Culham Science Centre, Abingdon, UK, UK
[8]Max-Planck-Institut for Plasma Physics, EURATOM Association, Greifswald, Germany
[9]FOM Institute DIFFER, Association EURATOM-FOM, Nieuwegein, The Netherlands
** See annex of F. Romanelli et al, "Overview of JET Results", (23rd IAEA Fusion Energy Conference, Daejon, Republic of Korea (2010)).*

Preprint of Paper to be submitted for publication in Proceedings of the
20th International Conference on Plasma Surface Interactions , Eurogress, Aachen, Germany
21st May 2012 - 25th May 2012

ABSTRACT

Divertor radiation profiles, and power and particle fluxes to the target have been measured in attached JET L-mode plasmas with carbon and beryllium/tungsten wall materials. In the beryllium/tungsten configuration, factors of 2 to 3 higher power loads and peak temperatures at the low field side target were observed in high-recycling scrape-off layer conditions, while in close-to-sheath-limited conditions almost identical plasmas were obtained. The 30% reduction in total radiation with the beryllium/tungsten wall is consistent with a reduction of carbon as the dominant impurity radiator; however similar ion current to the plates, emission from recycling neutrals and neutral pressures in the pumping plenum were measured. Simulations with the EDGDE2/EIRENE code of these plasmas indicate a reduction of the total divertor radiation when carbon is omitted, but significantly higher power loads in high-recycling and detached conditions are predicted than measured.

1. INTRODUCTION

Radiation from impurities in the Scrape-Off Layer (SOL) of tokamaks critically impacts the SOL power balance and is considered to induce detachment of the divertor plasma at lower upstream densities than in otherwise purely hydrogenic plasmas. Carbon (C), in particular, has shown to strongly radiate in the temperature range characteristic of the divertor SOL (i.e., 10 to 50eV), which lead to significant power losses upstream of the hydrogen ionisation front [1]. In turn, less power is subsequently conducted to the divertor target plates. The lack of significant radiation from impurities in the SOL in devices with metallic walls, such as ASDEX Upgrade and JET, was anticipated to produce higher heat fluxes to, and generally hotter plasma conditions in front of the target plates. Previous investigations in ASDEX Upgrade low confinement plasmas with tungsten (W) Plasma-Facing Components (PFCs) in the main chamber, and both C and W divertor plates showed, however, insignificant changes to the Low Field Side (LFS) divertor plasma fluxes and temperatures for identical upstream parameters [2]. It was speculated that the C that remained in the device after campaign-wise replacement of C PFCs over several years was sufficient to yield almost identical SOL conditions for the two divertor materials.

A more significant reduction of carbon in the plasma is anticipated in the JET ITER-Like Wall (ILW) where, in one single shutdown, all carbon PFCs (carbon fibre composite, CFC) were replaced with beryllium (Be) and W [3]. In the ILW the main chamber walls consists of beryllium: bulk Be in high heat flux areas, such as limiters, and Be-coated CFC surfaces in the other, recessed areas. The divertor PFCs are made of bulk W at the horizontally inclined tiles at the LFS (tile 5 in ref. [4], the dominant strike zone) and W-coated CFC surfaces in the all the other divertor areas, including the vertically inclined High Field Side (HFS) target (tile 3 in ref. [4]). Sets of reference plasmas were established in the carbon wall configuration to facilitate direct comparison of plasmas to be obtained in the ILW [4]. This publication focuses on the comparison of a set of low-triangularity plasmas in low confinement (L-mode) conditions for a range of upstream densities in the C and ILW configurations. These plasmas were analysed for radiative losses in the SOL, particle and heat

fluxes to the divertor target plates, and the electron temperature at the LFS plate. The experimental studies are complemented by numerical assessment of the absence of C as the dominant radiator in the SOL by simulating these plasmas with the fluid edge code EDGE2D/EIRENE [5], [6].

2. COMPARISON OF L-MODE PLASMAS IN THE CARBON AND ILW CONFIGURATION

2.1. DESCRIPTION OF REFERENCE PLASMAS

Extensive characterisation of the SOL conditions in both material configurations was obtained at the LFS midplane region, in the HFS and LFS divertor legs, and along the HFS and LFS target plates in low-triangularity ($\delta \sim 0.2$) plasmas with the HFS strike point on the HFS vertical plate (tile 3) and the LFS strike point on the horizontal plate (tile 5). The experiments were conducted at machine parameters typical for JET: plasma current, I_p, of 2.5MA, toroidal field, B_T, on the magnetic axis of 2.5 T, resulting in an edge safety factor, q_{95}, of 3.4. Low-power, neutral beam injection (1.6MW) was applied to obtain stationary L-mode conditions and to enable ion temperature and impurity density measurements. Together with ohmic heating, the total input power ranged from 2.8 to 3.0MW (Fig.1a). During current flattop the upstream density (core and edge line-averaged, pedestal, and SOL at the LFS midplane) was raised step-wise by deuterium gas fuelling from the top and divertor regions and held constant for 4 to 5 s to incorporate strike point sweeps of the order 1 to 2cm for diagnostic purposes. In the C wall, line-averaged densities corresponding to 22%, 34%, and 38% of the Greenwald density (n_{GW} [7]) were achieved, resulting in attached plasma conditions in both divertor legs before the ion current rollover [8]. In the ILW, attached and fully detached divertor conditions in both divertor legs were achieved in gas fuelling ramps and steps from the lowest permissible density to the density limit: here, fractions of n_{GW} ranged from 21% to 65%, while the density limit was obtained at 69% of n_{GW}.

2.2. RADIATIVE LOSSES IN THE SOL

In both materials configuration the total radiative power, P_{rad}, integrated over the core plasma, main chamber SOL, and divertor SOL increased linearly with upstream density (Fig.1a); within the limited data set the increase is slightly steeper in the C device than in the ILW. The total radiative power was measured by bolometry, and 2-D poloidal profiles were obtained by tomographic reconstructions [9]. Integration over the divertor legs below the X-point indicates that with the C wall the total radiation in both divertor legs, $P_{rad,div}$, as well as in each leg separately, $P_{rad,HFS\ div}$ and $P_{rad,LFS\ div}$, saturated before the rollover of the ion current at the LFS plate (Fig.2b). In contrast, a continuous increase in P_{rad} with upstream density was observed in the ILW until the ion current to the LFS plate rolled over: at this upstream density $P_{rad,HFS\ div}$ saturated (Fig. 1b). $P_{rad,LFS\ div}$ saturated at about 30% higher upstream density than $P_{rad,HFS\ div}$. Spatial integration of the divertor regions is, however, very sensitive to the assumed boundary between the divertor and main SOL: integration over the divertor regions including the X-point and the lower part of the main SOL does not show

the reduction of $P_{rad,div}$ for the carbon wall case at the highest upstream density. This observation is consistent with 2-D measurements of low charge state C emission in JET [10] and DIII-D [11] showing the radiation extending in the HFS main SOL. Including the lower part of the main SOL on both the HFS and LFS the data indicate that $P_{rad,div}$ was about 30% higher in the C device than in the ILW. These numbers are consistent with initial measurements of the emission from low charge state C in the LFS divertor, and across the core and pedestal regions showing that carbon was reduced by about an order of magnitude in the ILW compared to the C wall [12]. Similarly, by going from the carbon wall to the ILW the effective charge state, Z_{eff}, was reduced from 1.6 to 1.4 at the lowest, and from 1.4 to 1.1 at medium upstream densities.

At the lowest upstream densities the power conducted to the LFS plate ($P_{div,LFS}$) is identical in the C and ILW configurations, whereas at the highest density obtained in the C wall, the $P_{div,LFS}$ is about a factor of 2 lower in C configuration (Fig.1c). The conducted power to the HFS plate ($P_{div,HFS}$) was measured in the C wall configuration only. These power loads were obtained by infrared thermography validated against thermocouple data [13]. This dependence is further indicative for more power being radiated in the divertor and main SOL in the C wall case due to the absence of C as the dominant radiator, as expected.

2.3. UPSTREAM AND DIVERTOR PLASMA CONDITIONS

To further elucidate the link between plasma conditions at the divertor plate and those upstream at the separatrix, the upstream electron density at the LFS midplane ($n_{e,sep,LFS-mp}$) was regressed against the line-averaged density ($<n_e>_{l,edge}$) in the edge/pedestal region, revealing a 1:2 dependence between these two parameters (Fig. 2a). Here, we benefitted from significantly improved profile data in the LFS pedestal and SOL regions from high-resolution Thomson scattering [14], a Li beam system [15], and a reciprocating probe [16]. The transformation from $<n_e>_{l,edge}$ to $n_{e,sep,LFS-mp}$ is significantly more uncertain due to ambiguities in the separatrix position from the magnetic equilibrium reconstructions. The upstream profiles for the lowest density case (only) were therefore shifted radially outward (by ~ 1.2 cm at the LFS midplane against the assumed position from the Li beam system) until electron pressure balance was obtained between the LFS strike point and the LFS midplane. All the other profiles at higher upstream density were shifted by the same amount. Nearly identical (within 50%) ion currents to the HFS and LFS plates ($I_{div,HFS}$ and $I_{div,LFS}$, respectively) were measured (by wedge-type target Langmuir probes [17], [18]) in attached conditions in the C and ILW configuration (Fig.2b). In the ILW, $I_{div,HFS}$ and $I_{div,LFS}$ continue to rise and saturate halfway through the scanned density range. When raising the upstream density step-wise and holding it for a few seconds, the rollover of $I_{div,HFS}$ and $I_{div,LFS}$ occurred at the same upstream density. In addition, data from the fuelling ramp show a distinct reduction in both $I_{div,HFS}$ and $I_{div,LFS}$ indicating a transition to partial detachment at either strike point: like in the steady-state fuelling cases, the transition in $I_{div,HFS}$ and $I_{div,LFS}$ occurred at the same upstream density.

While at the lowest upstream density identical peak electron temperatures were measured at the

LFS plate ($T_{e,peak,LFS\ plate}$) for the two materials configurations, factors of 2 to 3 higher temperatures were observed in the ILW at higher upstream densities (Fig.2c). This observation is consistent with the higher power loads in the ILW described in the previous section. For the ILW case the reduction of $T_{e,peak,LFS\ plate}$ from 25eV to 8eV coincides with the rollover of $I_{div,LFS}$. The neutral densities in divertor legs as indicated by low Balmer line emission of deuterium atoms and the neutral pressure measured in the divertor pumping plenum (data not shown) continue to rise during the rollover of $I_{div,LFS}$, and only saturate at the highest upstream densities obtained.

3. EDGE2D/EIRENE SIMULATIONS OF FUELLING RAMPS WITH THE CARBON AND ILW WALLS

3.1. SETUP OF SIMULATIONS

Utilising the experimental data at the LFS midplane, the 2-D multi-fluid edge code EDGE2D coupled to the neutral Monte Carlo code EIRENE was exercised to predict the same divertor parameters as obtained experimentally. The two material configurations were adapted as they were, including Be in main chamber and W in the divertor for the ILW [19]. Carbon as a third impurity species in the Be/W simulations was not invoked. The simulations were executed on two sets of grids: (a) two separate grids corresponding to the magnetic configurations of the actual pulses, and (b) one common grid corresponding to the ILW magnetic configuration. A detailed description of the code setup is given in [19]. It is important to note that cross-field drifts ($\mathbf{E}\times\mathbf{B}$ and $\mathbf{B}\times\nabla B$) are not included in these simulations; hence, the analysis focuses on the LFS divertor only.

By raising the fuelling rate continuously from the lowest rate up to rates corresponding to the density limit, as reported here, produces sets of quasi steady-state solutions. In addition, fully converged solutions were obtained at densities corresponding to the experimental values of $n_{e,sep,LFS-mp}$. The injection and pump locations were adapted as in the experiments: deuterium molecules are injected either at the top (C wall case) or divertor (ILW case), and removed in the corners of the divertor. For most cases the standard EIRENE model in the code package was used, while for few dedicated case a more extensive EIRENE model was explored [20], [21] which includes a more extensive set of elastic and inelastic collisions between deuterium ions and molecules, and molecular dissociation of D_2, and thus represents a better description for detached divertor conditions.

3.2. DEPENDENCE OF RADIATIVE POWER LOSSES ON WALL MATERIALS AND UPSTREAM DENSITY

The predicted total radiation in the pedestal and SOL regions, $P_{rad,ped+SOL}$, shows a similar monotonic increase with upstream density as the measured $P_{rad,ped+SOL}$, but generally underestimates the measurements by factors of 2 to 3 (Fig. 3a). For the C wall case, the predicted $P_{rad,ped+SOL}$ may be increased by raising the chemical sputtering yields above those given by Roth et al. [22]; however, in doing so the solutions then overestimate emission from low charge state C in the LFS divertor. Assuming higher power outflow from the core, similar to those in the experiments, does not change

the predicted $P_{rad,ped+SOL}$ significantly. Spatially, P_{rad}, is dominated by radiation from the divertor: $P_{rad,div}$ is approximately 30% higher in C wall than in the ILW case, as seen experimentally.
Splitting the total radiated power in its components, the simulations indicate that in the C wall case $P_{rad,ped+SOL}$ is dominated by C radiation for low-to-medium upstream densities, and equally shared by D and C radiation for densities above I_{div} rollover (Fig. 3b and c). For the ILW case, however, D radiation is predicted to dominate the total radiation over the entire density range achieved, as expected: the radiation potential of Be is a ten-times lower than for C [23]. W sputtering is completely suppressed at T_e below 30 eV at the targets, thus W radiation does not play a role in high-recycling and detached conditions. When comparing the C and ILW cases, 50 to 100% higher D radiation is observed for the ILW at medium to high upstream densities, whereas at the lowest density, D radiation is found to be similar. In these simulations the density limit was reached at higher upstream densities in the ILW, which is not seen experimentally [24].

To address this latter result, simulations were run on one single grid with exactly the same input parameters and wall definition assuming pure D, D and C with a C wall, and D and Be with the IWL wall. Qualitatively, they show similar functional dependences on upstream density as the cases run on separate grids. However, the D+C case reaches the density limit at 10% lower upstream densities than the pure-D and D+Be due to C radiation in the divertor, qualitatively similar to the experimental results. Because of these increased power losses, lower target temperatures are obtained at the LFS plate for the same upstream density, and the integral D radiation is lower at high densities. Very similar results were obtained for the pure-D and D+Be cases. Also, the location of D fuelling, i.e., top versus private flux region, showed to have a negligible effect. Hence, the differences seen in the cases run on separate grids appear to point to how the pump was implemented in the grid, which resolution requires further investigations.

3.3. DEPENDENCE OF P_{DIV}, I_{DIV}, AND $T_{E,PEAK}$ AT THE LFS ON WALL MATERIALS AND UPSTREAM DENSITY

Despite underestimating the total radiated power in the divertor, the predicted total power to the LFS target plate, $P_{div,LFS}$, is also underestimated by the simulations (Fig.4a). Within the uncertainties of the power flowing across the core-pedestal boundary, $P_{div,LFS}$ is 50 – 100% lower than the measurements at the lowest upstream density. At higher upstream densities the simulations are within 50% of the experimental data for the C wall case, and an order of magnitude lower than the data for the ILW case.

The functional dependence of the ion current to the LFS plate, $I_{div,LFS}$, with upstream density shows a more distinct peak at medium density for the ILW than for the C wall case (Fig. 4b). However, none of the simulations with the standard EIRENE model show the factor of 5 to 10 reduction in $I_{div,LFS}$ at the highest upstream densities observed experimentally for the ILW.

With increasing upstream density, and thus increasing divertor radiation, the peak electron temperature at the LFS plate continuously decreased, dropping below 2eV at upstream density

corresponding to the saturation of $I_{div,LFS}$ (Fig.4c). The simulations consistently overestimate $T_{e,peak,LFS}$ by about 20% for the C wall, and raising the power across the core-pedestal interface moves the calculated solution further away from the experimental data. For the ILW case, the predictions reproduce the measurements; at the highest upstream densities the predicted T_e across the plate is of the order 1eV, which is experimentally challenging to measure with Langmuir probes.

By extending the EIRENE model to include a more extensive set of elastic and inelastic collisions between deuterium ions and molecules, and molecular dissociation of D_2, a significant improvement of the match to the experimental $I_{div,LFS}$ at the high-density end was achieved (see also [21]). Including these physics produces a two-fold reduction of $I_{div,LFS}$, and $T_{e,peak,LFS}$ of the order 0.5eV (Figs.4b and c). In the low and intermediate density range, it leads to a 50% in the power to the LFS plate. It is mainly the reduction in temperature that produces the more pronounced drop in $I_{div,LFS}$ with the extended EIRENE model.

SUMMARY AND DISCUSSION

A comparison of the measured 2-D radiation profiles, and the power and particle loads to the divertor plates in attached L-mode plasma in the JET C and ILW material configurations showed the following characteristics:

(a) a 30% decrease in total radiation in the divertors in the ILW, consistent with a reduction the low-charge state C emission by an order of magnitude, and Z_{eff},

(b) similar conducted power to the LFS plate for nearly sheath-limited SOL conditions, and an increase by a factor of 2 in high-recycling conditions in the ILW,

(c) similar plate-integrated ion currents to the HFS and LFS plates,

(d) similar peak electron temperatures at the LFS plate for nearly sheath-limited SOL conditions, and factors of 2 to 3 higher temperatures in high-recycling conditions in the ILW

These observations, together with power load measurements, indicate that carbon in the divertor SOL significantly cools the plasmas in high-recycling, and likely also in detached conditions. The target materials appear to have a less significant impact on the ion and recycling fluxes, and the neutral densities.

Simulations of upstream density scans with the EDGE2D/EIRENE code qualitatively show that, run on the same simulation grid, the presence of C (and C radiation) leads lower $P_{div,LFS}$ and $T_{e,peak,LFS}$, and to a 10% lower density limit. Quantitatively, and using the actual magnetic equilibria and walls, the agreement with the experimental data is limited: both the radiated power and the power conducted to the LFS plates are underestimated by up to factors of 2 to 3. This is particular troubling for the ILW configuration since Be is a poor radiator and W is suppressed, hence power and momentum loss due to deuterium must play a bigger role than predicted. A more pronounced rollover and reduction of $I_{div,LFS}$, as well as $T_{e,peak,LFS} \sim 0.5$eV were achieved by including more collision reactions and molecular dissociation of D_2 in EIRENE.

ACKNOWLEDGMENT

This work was supported by EURATOM and carried out within the framework of the European Fusion Development Agreement (EFDA). The views and opinions expressed herein do not necessarily reflect those of the European Commission.

REFERENCES

[1]. M.E. Fenstermacher et al., Physics of Plasmas **4** (1997) 1761.
[2]. M. Wischmeier et al., Journal of Nuclear Materials **390-391** (2009) 250.
[3]. G.F. Matthews et al., Physica Scripta 2011 (2011) 014001.
[4]. S. Brezinsek et al., Journal of Nuclear Materials **415** (2011) S936.
[5]. R. Simonini et al., Contribution to Plasma Physics **34** (1994) 368.
[6]. D. Reiter et al., Journal of Nuclear Materials **196–198 (**1992**)** 80.
[7]. M. Greenwald et al., Nuclear Fusion **28** (1988) 2199.
[8]. M. Groth et al., Journal of Nuclear Materials **415** (2011) S530.
[9]. A. Huber et al., Fusion Engineering and Design **82** (2007) 1327.
[10]. A. Huber et al., Journal of Nuclear Materials **313-316** (2003) 925.
[11]. M. Groth et al, Plasma Physics and Controlled Fusion **53** (2011) 124017.
[12]. S. Brezinsek et al., this conference.
[13]. T. Eich et al., Journal of Nuclear Materials **415** (2011) S856.
[14]. M.N. Beurskens et al., Nuclear Fusion **48** (2008) 095004.
[15]. M. Brix et al., submitted to Review of Scientific Instruments May 2012.
[16]. C. Silva et al., this conference.
[17]. R.D. Monk et al., Journal of Nuclear Materials **241-243** (1997) 396.
[18]. S. Marsen et al., this conference.
[19]. D. Harting et al., this conference.
[20]. S. Wiesen, EDGE2D/EIRENE code interface report, JET ITC-Report, http://www.eirene.de/e2deir_report_30jun06.pdf (2006).
[21]. C. Guillemaut et al., this conference.
[22]. J. Roth et al., Nuclear Fusion **44** (2004) L21.
[23]. Atomic Data and Analysis Structure 1995-2008, http://adas.phys.strath.ac.uk.
[24]. A. Huber et al., this conference.

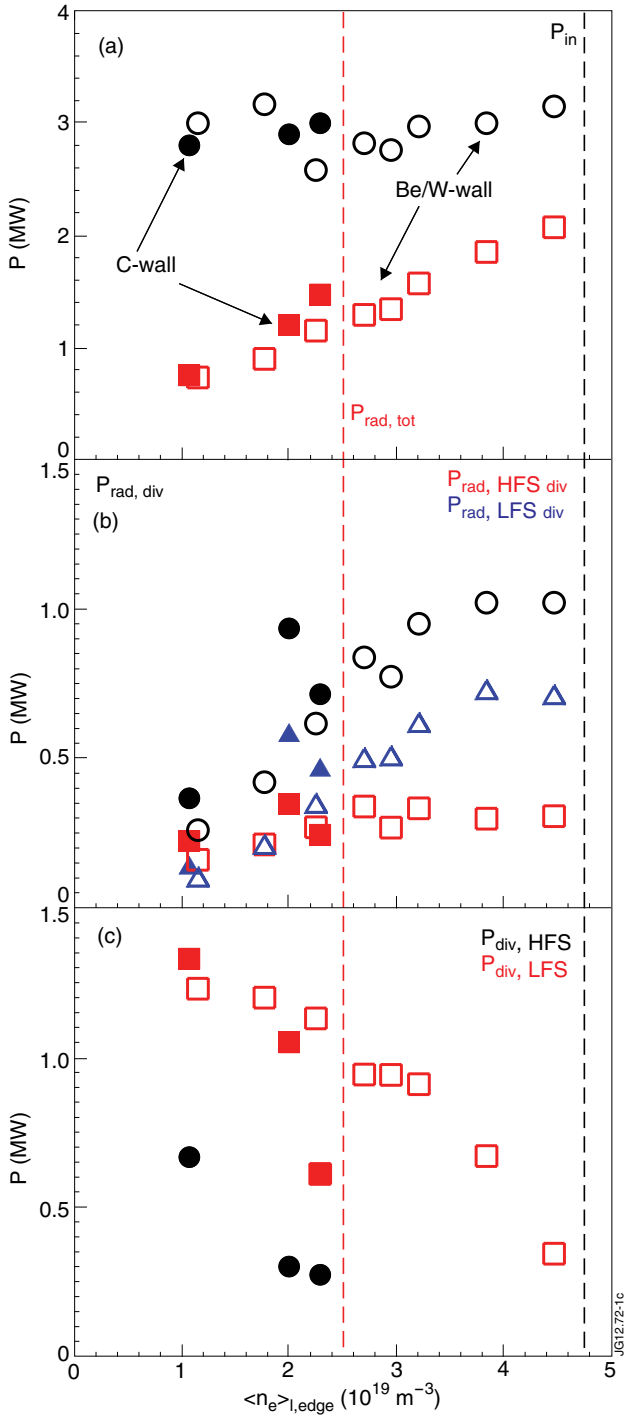

Figure 1: (a) Total input power (P_{in}, black circles) and radiated power ($P_{rad,tot}$, red squares), (b) radiated power in the divertor (black circles), separated into HFS (red squares) and LFS (blue triangles), and (c) conducted power to the HFS (black circles) and LFS plates (red squares) as function of line-averaged edge density. The solid and open symbols refer to the carbon wall and ILW configurations, respectively. The black vertical line indicate the density limit, and the red vertical line the rollover of the ion current to the LFS plate.

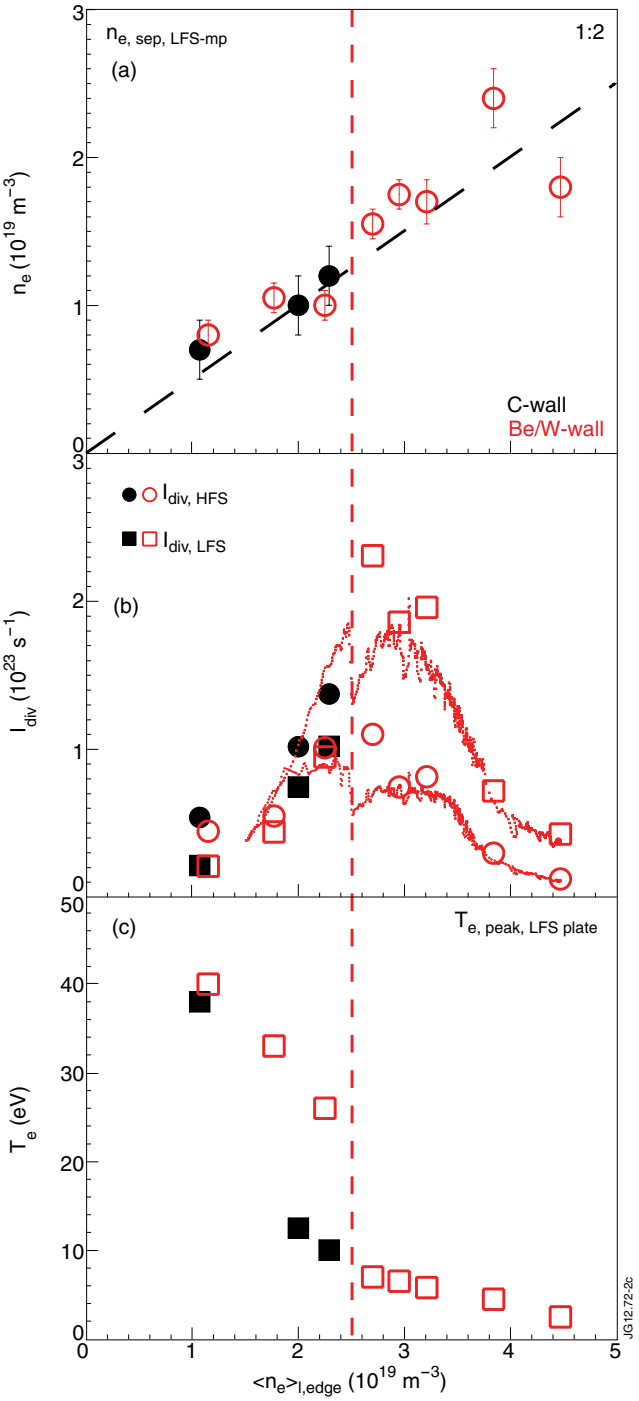

Figure 2: (a) Separatrix density, (b) total ion current to the HFS (circles) and LFS plates (squares), and (c) the peak T_e at the LFS plates as function of line-averaged edge density. The solid and open symbols refer to the carbon wall and ILW configurations, respectively. The small red dots in (b) show I_{div} taken during a continuous fuelling ramp. The vertical line marks the rollover of $I_{div,LFS}$.

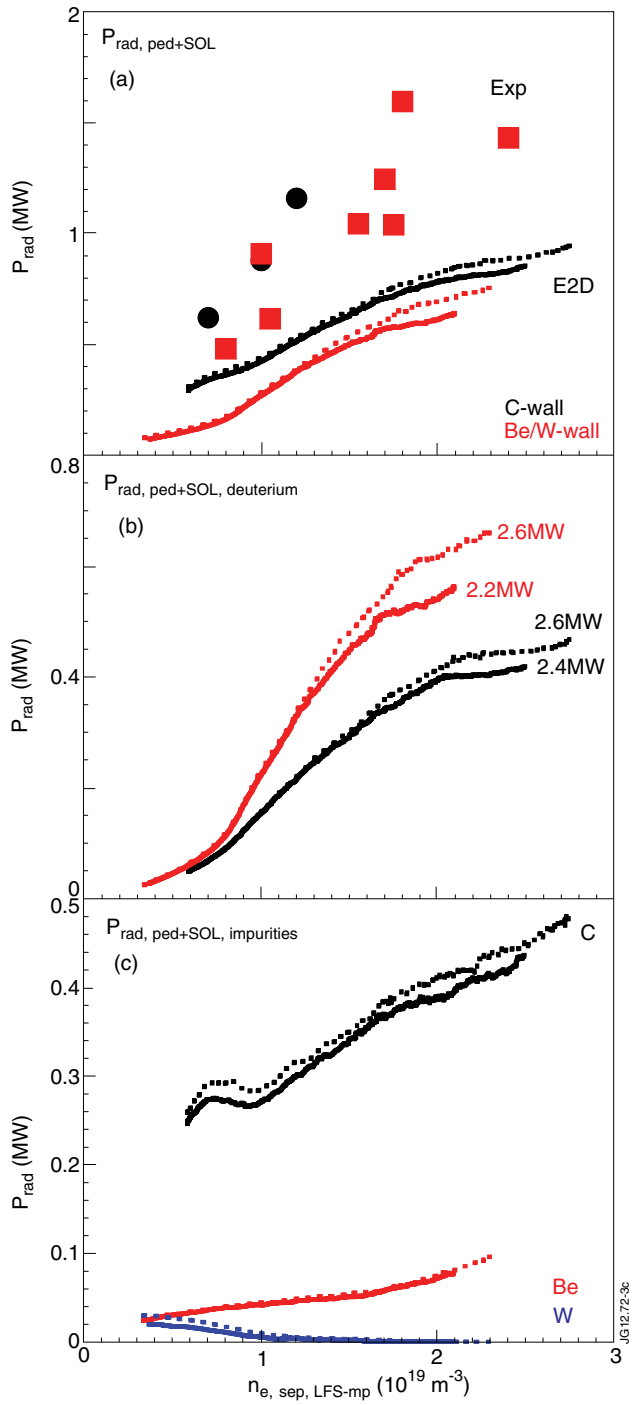

Figure 3: (a) Total radiated power in the pedestal and SOL regions, and separated into deuterium radiation (b) and impurity radiation (c) as a function of separatrix density at the LFS midplane. In (a), the symbols represent the experimental measurements in the carbon (black) and ILW (red) configurations. EDGE2/EIRENE simulations (lines) were executed with powers across the core-pedestal interface corresponding to the lowest (solid lines) and highest power (dashed lines) as derived from the experiments.

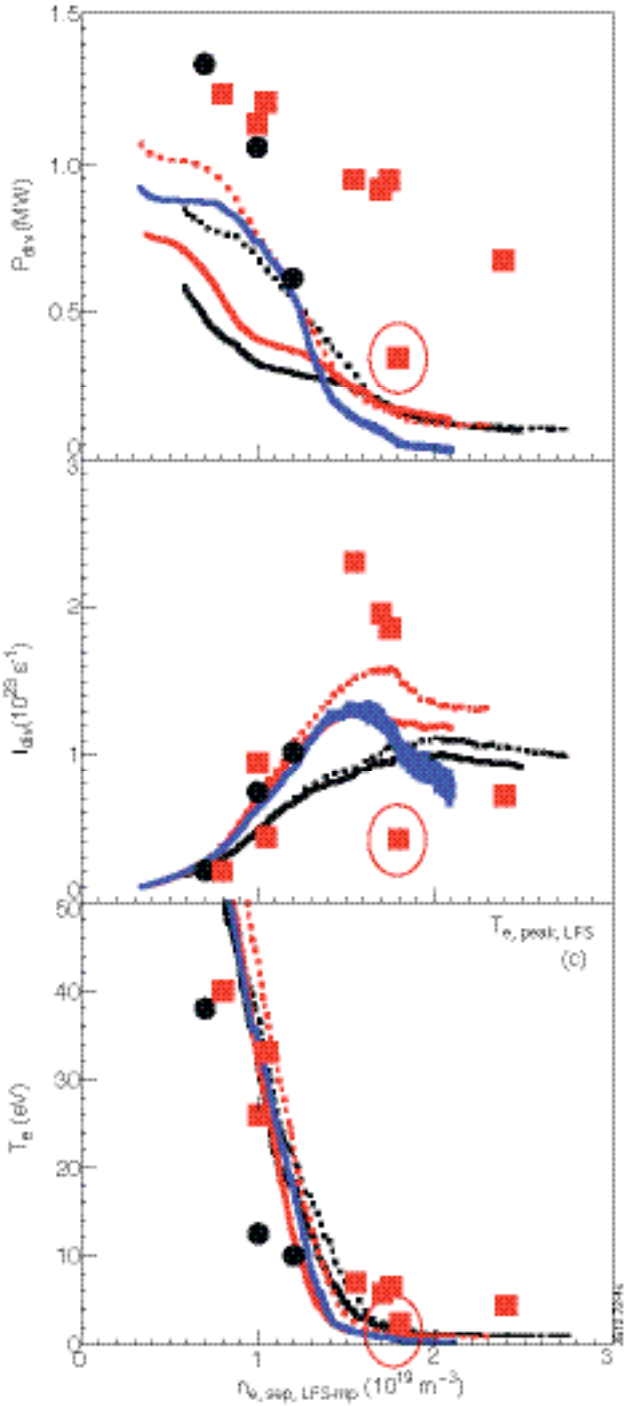

Figure 4: Total conducted power (a) and ion current (b) to the LFS plate, and the peak T_e at the LFS plate (c) as a function of separatrix density at the LFS midplane. The symbols represent the experimental measurements in the carbon (black) and ILW (red) configurations. EDGE2/EIRNEE simulations (lines) were executed with powers across the core-pedestal interface corresponding to the lowest (solid lines) and highest power (dashed lines) as derived from the experiments. The blue solid line shows the predictions using an extended EIRENE model.